0026-895X/96/051167-11$3.00/0

MOLECULAR PHARMACOLOGY, 50:1167–1177 (1996).

Three New Toxins from the Scorpion *Pandinus imperator* Selectively Block Certain Voltage-Gated K^+ Channels

ROBERT S. ROGOWSKI, JOHN H. COLLINS, THOMAS J. O'NEILL, THOMAS A. GUSTAFSON, TACO R. WERKMAN,[1] MICHAEL A. ROGAWSKI, TODD C. TENENHOLZ, DAVID J. WEBER, AND MORDECAI P. BLAUSTEIN

Departments of Physiology (R.S.R., T.J.O., T.A.G., M.P.B.), Biochemistry and Molecular Biology (J.H.C., T.C.T., D.J.W.), and Medicine (M.P.B.), School of Medicine, and the Medical Biotechnology Center, Biotechnology Institute (J.H.C.), University of Maryland, Baltimore, Maryland 21201, and Neuronal Excitability Section, Epilepsy Research Branch, National Institute of Neurological Disorders and Stroke, National Institutes of Health, Bethesda, Maryland 20892 (T.R.W., M.A.R.)

Received June 18, 1996; Accepted August 3, 1996

SUMMARY

Three 35-amino acid peptide K^+ channel toxins (pandinotoxins) were purified from the venom of the scorpion *Pandinus imperator*: the toxins are designated pandinotoxin (PiTX)-Kα, PiTX-Kβ, and PiTX-Kγ. In an ^{86}Rb tracer flux assay on rat brain synaptosomes, all three toxins selectively blocked the component of the K^+-stimulated ^{86}Rb efflux that corresponds to a voltage-gated, rapidly inactivating (A-type) K^+ current (IC_{50} = 6, 42, and 100 nM, respectively). These toxins blocked neither the noninactivating component of the K^+-stimulated ^{86}Rb efflux (corresponding to a delayed rectifier) nor the Ca^{2+}-dependent component of the ^{86}Rb efflux (i.e., a Ca^{2+}-activated K^+ current) in these terminals. PiTX-Kα, which was expressed by recombinant methods, also blocked the Kv1.2 channel expressed in fibroblasts (IC_{50} = 32 pM). PiTX-Kα and PiTX-Kβ have identical amino acid sequences except for the seventh amino acid: a proline in PiTX-Kα, and a glutamic acid in PiTX-Kβ. They have substantial sequence homology, especially at the carboxyl termini, with another scorpion toxin, charybdotoxin (ChTX), which blocks both the Ca^{2+}-activated and the rapidly inactivating, K^+-stimulated ^{86}Rb efflux components in synaptosomes and the Kv1.2 channel. PiTX-Kγ, however, has much less sequence homology. Conserved in all four toxins are three identically positioned disulfide bridges; an asparagine at position 30; and positive charges at positions 27, 31, and 34 (based on ChTX numbering). PiTX-Kγ is novel in that it has a fourth pair of cysteines. The PiTX structures were computer simulated, using ChTX as a model. We speculate that the three-dimensional structures of all three PiTXs resemble that of ChTX: a β-sheet at the carboxyl terminus, containing three cysteines, is linked to the central α-helix by two disulfide bridges (C17—C35 and C13—C33) and to an extended amino-terminal fragment by the third disulfide bridge (C7—C28). Further analysis of the three-dimensional structures reveals differences that may help to explain the selectivity and affinity differences of these toxins.

A number of short polypeptide toxins (37–39 amino acids) that are selective blockers of specific voltage-gated and Ca^{2+}-activated K^+ channels have been identified in recent years (1). These toxins, several of which have been purified from scorpion venoms, have aided in the characterization of the K^+ channels that serve as their acceptors (e.g., Refs. 2–5). Many peptide K^+ channel toxins from scorpion venom that have been studied (e.g., ChTX, margatoxin, noxiustoxin, and tityustoxin-Kα) seem to be readily reversible (6–9). In contrast, however, venom from the North African scorpion *Pandinus imperator* contains a component or components that block, with poor reversibility, voltage-gated, noninactivating (delayed rectifier) K^+ channels in bullfrog myelinated nerve fibers (10) and inactivating K^+ channels in GH_3 cells (11). The active K^+ channel toxins from this venom have not, however, previously been purified and characterized.

In an earlier report (12), we showed that venom from *P. imperator* selectively blocked a component of ^{86}Rb efflux from rat brain synaptosomes that could be ascribed to voltage-gated, inactivating (A-type) K^+ channels. This venom had a negligible effect on the two components of ^{86}Rb efflux, which we attribute to the Ca^{2+}-activated and voltage-gated, noninactivating K^+ channels. Here, we describe the purification, characterization, and primary structures of three peptides (PiTXs) from this venom that block the aforementioned component of ^{86}Rb efflux in synaptosomes. One of the toxins,

This work was supported by National Institutes of Health Grants NS16106 (M.P.B.) and GM52071 (D.J.W.), by a National Institute of Mental Health Grant to the Maryland Psychiatric Research Institute Neuroscience Center for Research in Schizophrenia (P50-MH44211; subproject director, M.P.B.), and by funds from the University of Maryland School of Medicine, the University of Maryland at Baltimore Graduate School, and the Medical Biotechnology Center of the University of Maryland Biotechnology Institute.

[1] Current affiliation: Department of Zoology, University of Amsterdam, Kruishaan 320, 1098 FM Amsterdam, The Netherlands.

ABBREVIATIONS: ChTX, charybdotoxin; α-DaTX, α-dendrotoxin; PiTX, pandinotoxin; SDS, sodium dodecyl sulfate; PAGE, polyacrylamide gel electrophoresis; HPLC, high performance liquid chromatography; EGTA, ethylene glycol bis(β-aminoethyl ether)-*N*,*N*,*N*′,*N*′-tetraacetic acid; HEPES, 4-(2-hydroxyethyl)-1-piperazineethanesulfonic acid; NH_4OAc, ammonium acetate.

PiTX-Kα, which we have studied most extensively, blocks, with very high affinity, the Kv1.2 channel stably expressed in fibroblasts as well as the synaptosome A-type K^+ channel. The other two PiTXs, which are present in similar abundance in the venom, also selectively block the synaptosome A-type K^+ channel.

The three PiTXs are 35 amino acids in length. Despite some novel features, all three PiTXs have significant sequence homologies to a number of other scorpion K^+ channel toxins (1). This enabled us to model the tertiary structures of the PiTXs and to speculate about the features of their three-dimensional structures that determine their acceptor site selectivity and affinity. All previously sequenced scorpion K^+ channel toxins contain three disulfide bridges (1). This is also true of two of the PiTXs. The third toxin, PiTX-Kγ, however, contains a fourth pair of cysteines. These two cysteines form a fourth disulfide bridge that apparently does not disrupt the conserved folding pattern that is expected as a result of the other three disulfide bridges.

Materials and Methods

Toxin purification. Toxins were purified from the venom of *P. imperator* by a two-step purification process as described previously (12). In brief, the toxins were extracted in 20 mM NH_4OAc (pH 6.8; 30 mg of venom/ml). The water-soluble toxins were separated by HPLC cation exchange using a linear NH_4OAc gradient from 0.02 to 1.0 M (Fig. 1). The individual toxins were then purified from the peaks of interest by reverse-phase HPLC (Fig. 2).

Protein concentrations were determined using the Pierce Micro BCA assay kit (Pierce Chemical, Rockford, IL). Toxin purity and approximate molecular weights were determined by SDS-PAGE (13), but final molecular weight determinations were obtained directly from the amino acid sequences of each of the prevalent toxins.

Amino acid sequencing. Amino acid sequences were determined by automated Edman degradation with an Applied Biosystems (Foster City, CA) model 477A sequencer equipped with an on-line amino acid phenylthiohydantoin analyzer. Standard protocols supplied by the manufacturer were used for analysis. Before sequencing, disulfide bridges were reduced with β-mercaptoethanol and then alkylated with 4-vinylpyridine according to the procedure described in Applied Biosystems User Bulletin No. 61, Cysteine residues were positively identified during sequencing as their pyridylethylcysteine phenylthiohydantoin residues.

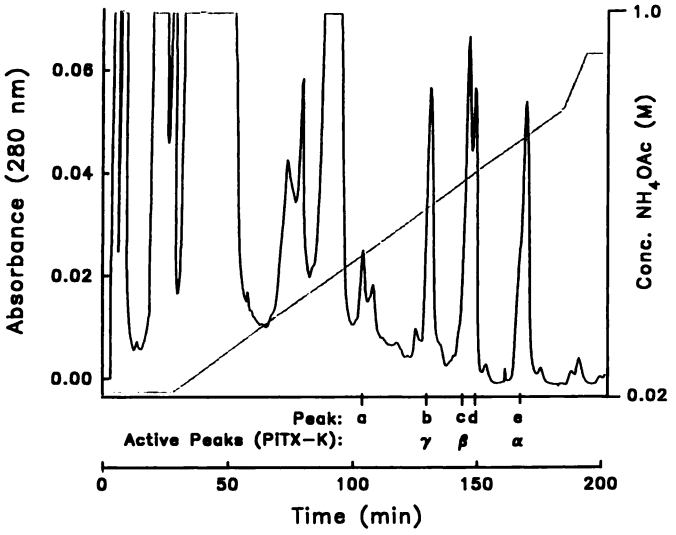

Fig. 1. HPLC cation exchange chromatogram of the water-soluble components of crude venom from the North African scorpion *P. imperator*. A linear gradient from 0.02 to 1.0 M NH_4OAc with a flow rate of 1 ml/min was used. *b–e*, Peaks of interest labeled inhibited K-stimulated ^{86}Rb efflux in synaptosomes.

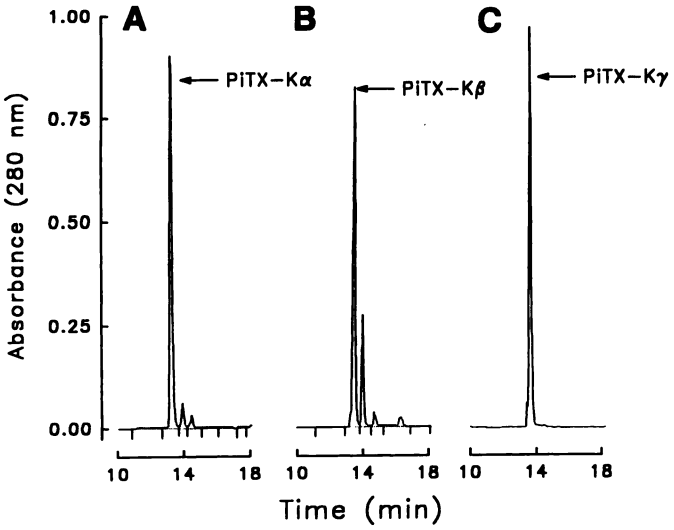

Fig. 2. Purification of PiTX-Kα, PiTX-Kβ, and PiTX-Kγ by reversed phase HPLC. A, Fraction *e* from the cation exchange step in Fig. 1. A 30-min linear gradient from 0.1% trifluoroacetic acid in water to 0.1% trifluoroacetic acid in acetonitrile was used with a flow rate of 1 ml/min. *Arrow*, the active peak, PiTX-Kα. B, Reversed phase of fraction *c* from the cation exchange step in Fig. 1 (same conditions as in A). *Arrow*, the active toxin, PiTX-Kβ. C, Reversed phase of fraction *b* from the cation exchange step in Fig. 1 (same conditions as in A). *Arrow*, the active toxin, PiTX-Kγ.

Expression of PiTX-Kα by recombinant methods. To express the 35-amino acid PiTX-Kα, two oligonucleotides were prepared (14, 15). The sequence of the sense strand oligonucleotide (shown 5′ to 3′) was CGCGGATCCGTCGACTACAAAGACGACGATGATAAAACTA-TCAGCTGCACTAACCCGAAACAATGCTACCCGCACTGTAAGA-AAGAAACTGGTTACCCG. The sequence of the antisense strand (5′ to 3′) was GCCGGAATTCAAGCTTCTAACGACCGAAGCATTTGC-ATTTACGATTCATGCATTTAGCGTTCGGGTAACCAGTT-TCTTTCTTACAG.

These oligonucleotides were designed so that they contained a 25-bp overlap at their 3′ ends. To construct a gene that encodes PiTX-Kα, the two oligonucleotides were annealed by mixing equimolar amounts of each, and they were extended by PCR. The extended product was then purified from agarose gels using the glass bead method of purification (Qiagen, Studio City, CA). The PCR product was digested with *Eco*RI and *Bam*HI, ligated into the pBluescript plasmid, and sequenced. The plasmid was then digested with *Sal*I and *Hin*dIII. The insert was ligated into the pSR9 expression plasmid (16), which had been digested with *Sal*I and *Hin*dIII. The final clone, termed pSR9.PiTX, was designed to produce a fusion protein containing T7 gene 9 sequences, the pFLAG epitope, and an enterokinase cleavage site linked to the toxin sequences. This expression vector therefore permits i) efficient induction of expression by T7 RNA polymerase, ii) increased fusion protein stability and solubility due to the gene 9 fusion sequences, iii) facile identification of the fusion protein during expression and purification using the anti-Flag M2 antibody (Kodak, Rochester, NY), and iv) efficient cleavage of the toxin from the fusion protein with enterokinase to yield an intact toxin amino terminus.

Molecular modeling of toxin structures. Beginning with the atomic coordinates for ChTX (17, 18), we used the programs CHARMm and QUANTA (Molecular Simulations, Burlington, MA) to obtain and view energy-minimized model structures for the three PiTXs in a similar manner to that previously described for other toxins (5, 19). The amino acid sequence for each toxin was entered

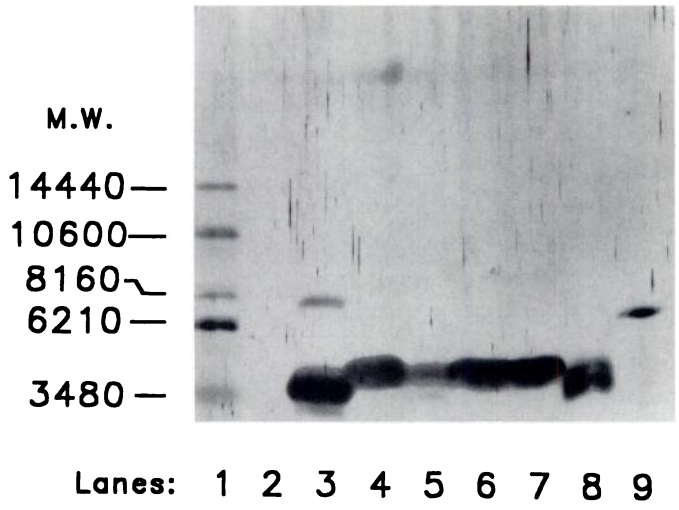

Fig. 3. SDS-PAGE of purified toxins from the venom of *P. imperator*. Each lane contains ≈100 ng of toxin. *Lane 1*, molecular mass standards; *lane 2*, blank; *lane 3*, peak *a* from the cation exchange column of Fig. 1; *lane 4*, PiTX-Kγ; *lane 5*, PiTX-Kβ; *lane 6*, Peak *d* from the cation exchange column Fig. 1; *lane 7*, PiTX-Kα; *lane 8*, tityustoxin-Kα (12); *lane 9*, α-DaTX (24). All three PiTXs had molecular masses of ≈4000 Da, which is close to the values determined from their amino acid sequences.

and then homology-modeled using the χ, ϕ, and ψ angles from ChTX as a starting point in the calculation. All amino acid residues, including proline residues, were assumed to be in the *trans*-configuration with protonation states based on pH 7.0. The resulting structures were subjected to 500 cycles of steepest descent energy minimization using CHARMm polar hydrogen force field parameters with a distance-dependent dielectric constant, followed by adopted-basis Newton-Rapheson minimization under the same conditions, until convergence was achieved (gradient tolerance = 0.01). As a control, the entire structure of ChTX was also subjected to energy minimization under the same conditions. Although the ChTX structure condensed somewhat, the overall structure was well preserved: root-mean-square deviation from published coordinates (17, 18, 20) was <2Å.

Assay of toxin activity in synaptosomes. A crude synaptosome (pinched-off presynaptic nerve terminal) preparation was obtained from homogenized rat forebrains. This preparation, which consisted of the pellet from the second 10,000 × *g* centrifugation (12, 21), was used for all ^{86}Rb flux assays.

Voltage-gated K^+ channels are nearly as permeable to Rb^+ as they are to K^+, and because of its much longer half-life, ^{86}Rb is a more convenient tracer than ^{42}K. Therefore, ^{86}Rb efflux was routinely used to measure synaptosome membrane conductance to K^+ (12, 21–23). The methods for loading synaptosomes with ^{86}Rb and for using an ^{86}Rb efflux assay to identify components of the efflux associated with A-type K^+ channels and delayed rectifier K^+ channels in synaptosomes have been described previously (12, 22, 24) and are illustrated in Results. To prevent the activation of Ca^+-activated K^+ channels, Ca^{2+}-free incubation solutions were used unless otherwise noted (12, 22, 24). The standard incubation solution (5K) contained 145 mM NaCl, 5 mM KCl, 0.1 mM RbCl, 2 mM $MgCl_2$, 10 mM glucose, 0.5 mM NaH_2PO_4, and 10 mM HEPES adjusted to pH 7.4 with NaOH. The depolarizing solution (100K) differed in that it contained 100 mM KCl and only 50 mM NaCl.

In brief, synaptosomes were preincubated in 5K solution (6–8 mg of protein/ml) containing ^{86}Rb (100 μCi/μmol of Rb) at 30° for 20 min. A 100-μl aliquot of the suspension was then diluted with 11.1 μl of 5K, which often contained toxins (see Results); the toxin concentrations, after dilution, are those indicated in Results. After an additional 15-min incubation, a 90-μl aliquot was diluted into 2 ml of 5K and filtered through a glass-fiber filter. The filter, containing trapped synaptosomes, was washed four times with 1.0-ml aliquots of toxin-free 5K; all wash filtrates, containing extracellular ^{86}Rb and unbound toxins, were discarded. The entire wash procedure was timed to take 10 sec. The ^{86}Rb-loaded synaptosomes on the filters were then incubated for 1–5 sec (timed with a metronome; see Results) with 1.0 ml of either 5K or 100K solution at 30°. ^{86}Rb efflux

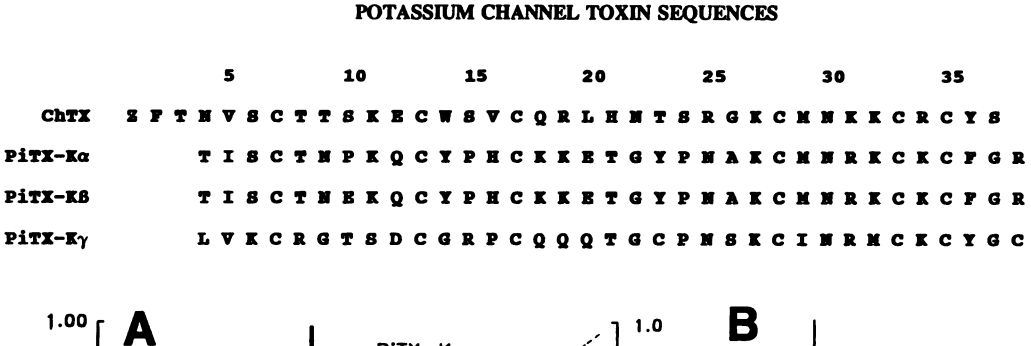

Fig. 4. Amino acid sequences of ChTX (40) and PiTX-Kα, PiTX-Kβ, and PiTX-Kγ. The toxins are aligned so that the six conserved cysteines lie in identical positions; the numbering corresponds to ChTX.

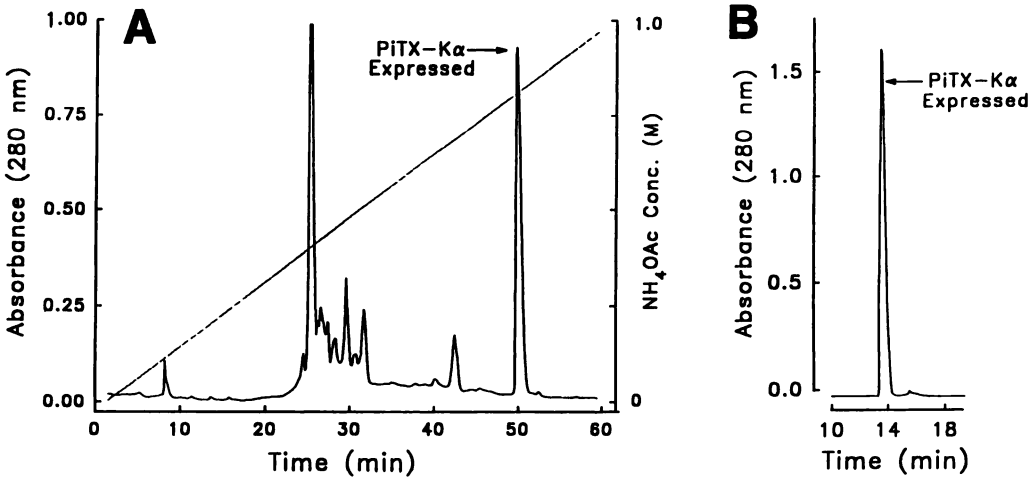

Fig. 5. Cation exchange (A) and reversed phase (B) HPLC purification of PiTX-Kα expressed by recombinant methods using a synthetic gene (see Materials and Methods). The conditions in A and B are the same as those used for native toxins (Figs. 1 and 2).

was terminated by the addition of 0.7 ml of a stop solution to the incubation medium and rapid filtration of all of the fluid; the ^{86}Rb both in the filtrate and on the filter were determined by liquid scintillation spectroscopy. The stop solution contained 145 mM tetraethylammonium chloride, 5 mM tetrabutylammonium chloride, 0.1 mM RbCl, 10 mM $MgCl_2$, 10 mM $NiCl_2$, and 10 mM HEPES titrated to pH 7.4. The effluxes are expressed as the fraction of the total (filter plus filtrate) counts that appeared in the filtrate. The K^+-stimulated ^{86}Rb efflux (ΔK) is the efflux into 100K minus the corresponding efflux into 5K. The increment in the ^{86}Rb efflux observed when 1.2 mM $CaCl_2$ was present in the 100K efflux solution corresponds to the Ca^{2+}-activated Rb efflux (ΔCa).

Electrophysiological studies. CL1023 cells (B82 fibroblast cells stably transfected with Kv1.2 K^+ channel cDNA) were grown in culture as described previously (7). Before recording, the culture medium was replaced with bathing solution containing 140 mM NaCl, 5 mM KCl, 2 mM $CaCl_2$, 1 mM $MgCl_2$, 5.6 mM D-glucose, and 5 mM HEPES, pH 7.4 (osmolality, 330–335 mOsM). Patch electrodes (2–4 MΩ) were pulled from filament-containing thin-wall glass capillary tubes (o.d., 1.5 mm; World Precision Instruments, New Haven, CT), heat polished, coated with Sigmacote (Sigma Chemical, St. Louis, MO), and filled with intracellular solution containing 150 mM KCl, 2 mM $MgCl_2$, 0.1 mM $CaCl_2$, 1.1 mM EGTA, and 5 mM HEPES, pH 7.2 (osmolality, 320–325 mOsM). Whole-cell recordings were obtained with an Axoclamp 2A amplifier (Axon Instruments, Burlingame, CA) in discontinuous single-electrode voltage-clamp mode (sampling rates, 15–23 kHz). Voltage-clamp pulses were generated and currents were acquired under computer control using an Axolab-1 interface with the CLAMPEX module of the pCLAMP software suite (Axon Instruments). Currents were low-pass filtered at 1 kHz. The CLAMPFIT program was used to measure the current level at the end of the voltage command pulses (steady state current).

PiTX-Kα stock solutions prepared in distilled water were diluted in bathing solution at the appropriate concentration immediately before the start of each experiment. Toxin-containing bath solutions were applied with a multibarrel rapid perfusion system at a flow rate of 0.5 ml/min; between toxin applications, the cell was perfused with bathing solution alone. In the concentration-response experiments, three toxin concentrations were examined for each cell. Before application of the lowest toxin concentration, five consecutive 1-sec depolarizing steps from −60 to +30 mV were applied at 20-sec intervals. At 2–3 min after the onset of perfusion with the lowest toxin concentration, an additional five steps were applied. After 5-min wash-out periods, the same protocol was repeated successively using the two higher toxin concentrations. The average of the steady state currents for each set of five pulses was used to calculate the percent of control values.

Statistical analysis. Averaged data are shown as mean ± standard error; the mean ± standard error for differences between two mean values (for the ΔK and ΔC ^{86}Rb effluxes) were calculated as described previously (25). Dose-response curves were fitted as described in the legends to the figures.

Results

Toxin purification and sequence determination. Separation of the water-soluble *P. imperator* venom components by cation exchange HPLC yielded three peaks (Fig. 1, *b*, *c*, and *e*), which inhibited the 100 mM K-stimulated ^{86}Rb efflux from synaptosomes (ΔK; see below). The active peptides (designated as PiTXs or PiTX-Kγ, PiTX-Kβ, and PiTX-Kα) in these three fractions were each purified to homogeneity by reverse-phase HPLC (Fig. 2, A–C). Approximately equal amounts of the three toxins were present in the crude venom (~10 μg/mg lyophilized venom). The homogeneity of the purified toxins was confirmed by SDS-PAGE analysis (Fig. 3). The material in peak *d* from the ion exchange column also

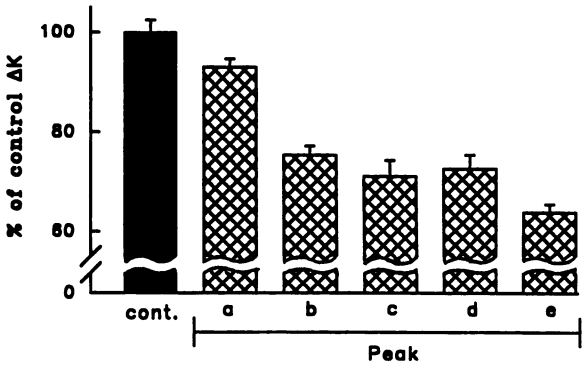

Fig. 6. Effects of reversed phase-purified toxins (100 nM each) from the ion exchange column fractions shown in Fig. 1 on the 5-sec K-stimulated ^{86}Rb efflux (ΔK) from synaptosomes. *Bars*, (± standard error) differences of the mean values of four replicates each in 5K and 100K.

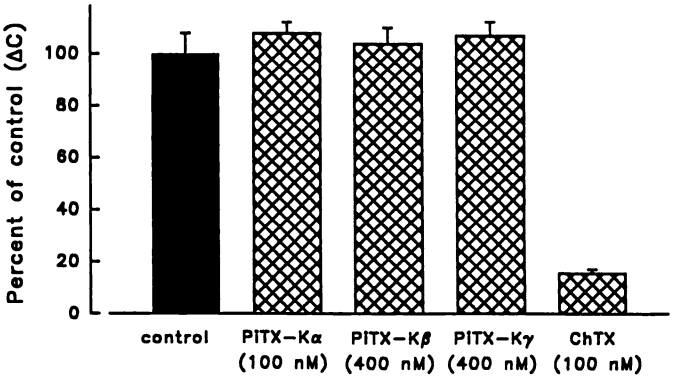

Fig. 7. Effects of the three PiTXs and ChTX on the Ca^{2+}-dependent, 100 mM K^+-stimulated component of ^{86}Rb efflux (ΔC) from synaptosomes. All solutions contained 10 mM 4-aminopyridine to block the voltage-gated inactivating and noninactivating K^+ channels. ΔC was calculated as the 5-sec ^{86}Rb efflux in 100 mM K^+ medium containing 1.2 mM Ca^{2+} minus the efflux in Ca^{2+}-free 100 mM K^+ medium, either with or without toxin. *Bars*, (± standard error) differences in the mean values of four replicates each in 100K and Ca^{2+}-free 100K.

inhibited ΔK (see below), but we obtained insufficient pure material to sequence completely. Because the apparent inhibitory potency of this material was lower than that of either PiTX-Kα or PiTX-Kβ, this compound was not further characterized.

The sequences of the three toxins are presented in Fig. 4, in which they are compared with ChTX. Note that PiTX-Kα and PiTX-Kβ differ from each another by a single amino acid in position 10 (using the numbering system for ChTX): a proline in PiTX-Kα and a glutamic acid in PiTX-Kβ. Also, like ChTX, both of these PiTXs have six cysteines (and three disulfide bridges), and they have more sequence identities to ChTX than does PiTX-Kγ. In addition, PiTX-Kγ has a fourth pair of cysteines and, except for the first three disulfide bridges (7–28, 13–33, and 17–35) and the region from amino acid 24 to 37, bears little sequence homology to the other PiTXs. A further analysis of toxin structure is presented below.

To obtain sufficient material for functional characterization, PiTX-Kα, the most potent of the three toxins (see below), was expressed in an *Escherichia coli* expression system (see Materials and Methods). The expressed toxin exhibited the same chromatographic characteristics as the native toxin (Fig. 5) and was fully active in the ^{86}Rb flux assay (see

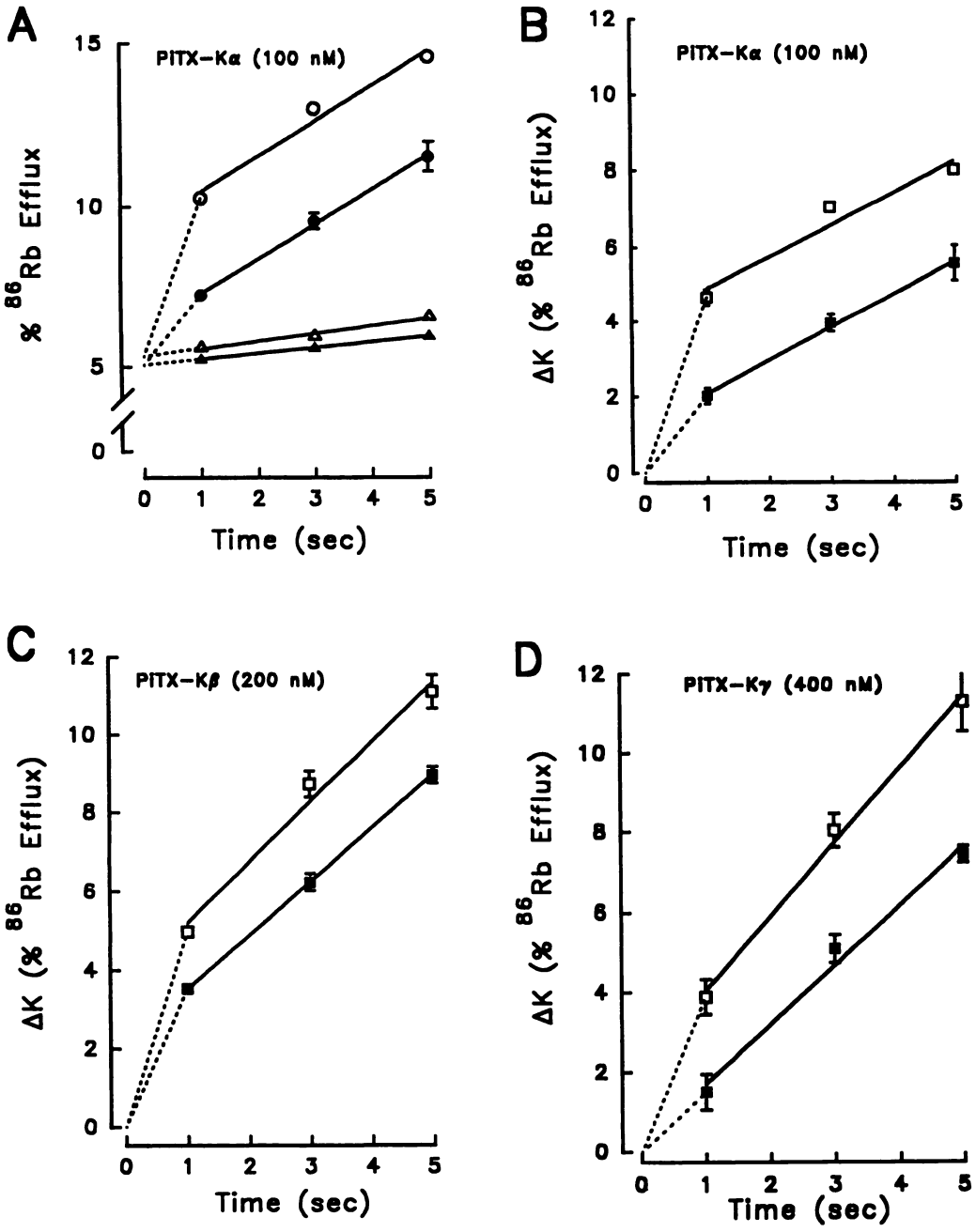

Fig. 8. Effects of PiTX-Kα, PiTX-Kβ, and PiTX-Kγ on the time course of ^{86}Rb efflux from rat brain synaptosomes in the absence of extracellular Ca^{2+}. A and A′, Effect of 100 nM PiTX-Kα. A, Effluxes into both 100 mM K^+ and 5 mM K^+ Ca^{2+}-free media. A′ (as in B and C), The ^{86}Rb efflux into 5 mM K^+ medium has been subtracted, showing only the K^+-stimulated ^{86}Rb efflux (ΔK). B, Effect of 200 nM PiTX-Kβ. C, Effect of 400 nM PiTX-Kγ. ○, ●, Efflux in 5 mM K^+ medium. △, ▲, Efflux in 100 mM K^+ medium. ○, △, and □, Toxins absent. ●, ▲, and ■, Toxins present. Values are the means of (A) five replicates and (B–D) differences in the means. *Standard error bars* are shown where they extend beyond the symbols.

below). Therefore, we will not distinguish between native and expressed PiTX-Kα in the ensuing discussion.

^{86}Rb efflux assay of purified PiTXs. The reversed phase-purified substances from each of the peaks of the ion exchange column (Fig. 1) were tested for their ability to inhibit the 100 mM K^+-stimulated ^{86}Rb efflux (ΔK) in synaptosomes. As shown in Fig. 6, a 100 nM concentration of each of these substances (from peaks *b–e*) inhibited ΔK by 25–35%. A maximum of ~35% inhibition of ΔK is observed with ChTX (not shown; see Ref. 24); this represents complete inhibition of the depolarization-activated, rapidly inactivating component of the ^{86}Rb efflux that apparently corresponds to the A-type K^+ channels (12, 26).

ChTX also blocks a Ca^{2+}-dependent component of the ^{86}Rb efflux (ΔCa) in synaptosomes (24). Previously, we reported that crude *P. imperator* venom had no effect on ΔCa (12). Fig. 7 shows that the purified toxins from peaks *b*, *c*, and *e* of the ion exchange column also had no effect on this ChTX-sensitive efflux component, which corresponds to the maxi Ca^{2+}-activated K^+ channel.

Fig. 8 illustrates the effects of the three purified PiTXs on the time course of ^{86}Rb efflux from synaptosomes. Fig. 8A shows the original data for the effect of PiTX-Kα on the efflux into both 5K and 100K solutions at 1, 3, and 5 sec: the toxin had a negligible effect on the efflux into 5K but markedly reduced the efflux into 100K at all three time points. The inhibition of the K^+-stimulated efflux (ΔK, which corresponds to 100K data minus the 5K data) by PiTX-Kα is shown in Fig. 8B. Comparable ΔK data for PiTX-Kβ and PiTX-Kγ are presented in Fig. 8, C and D; neither of these toxins significantly affected the efflux into 5K.

Extrapolation of the lines in Fig. 8, B–D, to time 0 (i.e., the

time at which 100K was introduced) indicates that all three toxins reduced the ordinate intercept. This indicates that the three PiTXs blocked a rapidly (<1 sec) inactivating component of the K^+-stimulated ^{86}Rb efflux, as we have observed with ChTX (24) and the snake toxin α-dendrotoxin (23). None of the PiTXs, however, affected the slope of the time course curve; this indicates that they did not block the component of ΔK that inactivates slowly (>5 sec). The latter is the component that is selectively blocked by tityustoxin-Kα and noxiustoxin (12); it may correspond to a delayed rectifier-type K^+ channel.

Fig. 9 shows the dose-response curves for the inhibition of ΔK by the three PiTXs. All three toxins blocked approximately one third of ΔK (5-sec incubation), which is the magnitude of the rapidly inactivating component of the 100K-stimulated ^{86}Rb efflux (12, 26). PiTX-Kα exhibited the highest affinity (IC_{50} = 6 nM), and there was no significant difference between the effects of the native and expressed toxins. The replacement of a proline at position 10 by a glutamic acid (Fig. 4: PiTX-Kβ), reduced the affinity 7-fold (IC_{50} for PiTX-Kβ = 42 nM). These IC_{50} values may be overestimates of the true IC_{50} values (i.e., the toxin affinities may be underestimated) if significant fractions of the toxin molecules dissociated from their binding sites during the 10-sec wash before introduction of the 100K efflux solution (see Materials and Methods).

PiTX-Kγ exhibited an even lower affinity block ($IC_{50} \approx$ 100 nM). In addition, the dose-response curve was somewhat less steep than those of the other two PiTXs (Fig. 9, ◆). This implies that it may interact with the K^+ channel in a somewhat different manner than PiTX-Kα and PiTX-Kβ.

Effects of PiTX-Kα on the current carried by Kv1.2 channels. Whole-cell voltage-clamp recordings were carried out on CL1023 fibroblast cells transformed to stably express the Kv1.2 K^+ channel. As illustrated in Fig. 10A, step depolarization of the cells from −60 to +30 mV evoked a slowly activating outward K^+ current that inactivated only minimally during the 1-sec step. PiTX-Kα produced a potent, concentration-dependent block of the K^+ current with nearly complete suppression of the current at a concentration of 1 nM.

The concentration dependence of block was examined in greater detail in a series of experiments with toxin concentrations of 3 pM to 1 nM. The mean percentage of control K^+ current at each toxin concentration is plotted in Fig. 10B. These values were well fit by the logistic function for a 1:1 binding model with an IC_{50} value of 32 pM.

The time course for the onset and recovery from block is illustrated in the experiments of Fig. 10, C–F. Block developed rapidly during the initial 20–40 sec of toxin application. Partial recovery occurred with a single exponential time course during the 4–5-min period after completion of the toxin exposure. The rate of recovery (mean rate constant ≈ 0.01 sec^{-1}) was independent of the toxin concentration.

Molecular modeling of PiTXs. The solution structures of ChTX and several homologous scorpion venom K^+ channel toxins have been determined by NMR spectroscopy (5, 17, 18, 27–29). The backbone fold for all of these toxins is virtually identical. Thus, the channel selectivity of scorpion toxins is most likely due to differences in side chains and surface charge, as is the case for the conotoxins (30). With this in mind, we created homology models based on the three-dimensional structure of ChTX, and we subjected them to energy minimization using the CHARMm polar hydrogen force field. Two views of each modeled PiTX structure and the NMR structure of ChTX are shown in Fig. 11, which illustrates the surfaces of the toxins that are most likely to face the extracellular fluid and the docking site in the external vestibule of the channel, respectively (1, 2, 4).

The current structural model for the ChTX block of K^+ channels is based on mechanistic and mutagenic analyses of toxin/channel interactions (2, 4, 9, 31, 32). The results of these studies suggest structural features such as i) shape complementarity of the toxin to the channel, ii) 4-fold symmetry in the four α subunits of the channel (assuming homotetrameric K^+ channels, which may be an oversimplification for many native K^+ channels), and iii) a role for the ϵ-amino group of the Lys27 of the toxin, which is believed to insert into the K^+ channel pore at the bottom of the external vestibule (2, 4, 31, 32). All three PiTXs have a large number of sequence identities to ChTX, including a lysine in a position homologous to Lys27 of ChTX (Figs. 4 and 11). Therefore, a similar pore occlusion model is proposed for channel blocking by the PiTXs (Fig. 12).

In Fig. 11, the bottom view of each toxin is oriented so that the critical lysine residue (Lys27) is located at the center, as if it were projecting out of the plane of the paper and into the pore of a K^+ channel. The other view is a top-down view illustrating residues that probably face the extracellular medium and do not interact with the channel. In contrast to ChTX, the PiTXs have three fewer residues at the amino terminus and therefore lack the first amino-terminal strand of the β sheet. The absence of these residues results in toxins that present a smaller surface area for interaction with the channel vestibule. Specifically, Pyro1Glu1 and Phe2 of ChTX

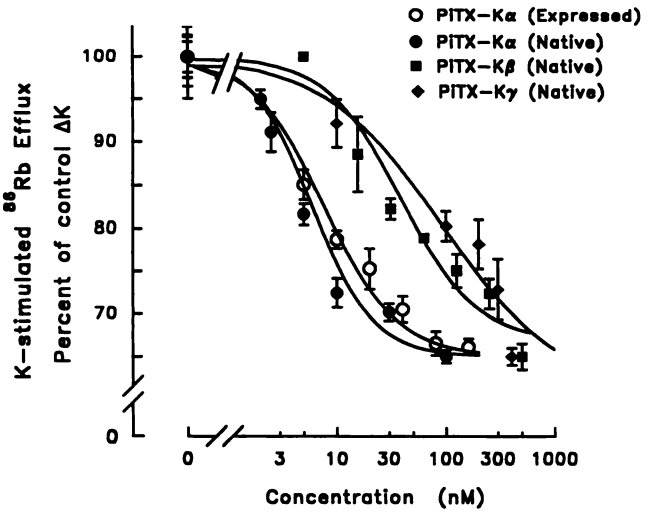

Fig. 9. Dose-response curves illustrating the effects of PiTX-Kα, PiTX-Kβ, and PiTX-Kγ on the 5-sec K^+-stimulated ^{86}Rb efflux in synaptosomes. Data for both native and expressed PiTX-Kα are shown. Thirty-five percent inhibition of control ΔK corresponds to complete block of the voltage-gated, rapidly inactivating component (12). The respective IC_{50} values for block of this component were 6 nM PiTX-Kα (both native and expressed), 42 nM PiTX-Kβ, and 100 nM PiTX-Kγ. *Symbols*, (mean ± standard error) differences of the mean values of four replicates each in 5K and 100K; *curves*, fit to the data *points* with SigmaPlot software using the equation: Percentage of control $\Delta K = 100/\{1 + ([toxin]/IC_{50})^{n_H}\}$, where [toxin] is the toxin concentration and n_H is the Hill coefficient. The values of n_H were 1.4, 1.0, and 0.9 for PiTX-Kα, Pi-Kβ, and Pi-γ, respectively.

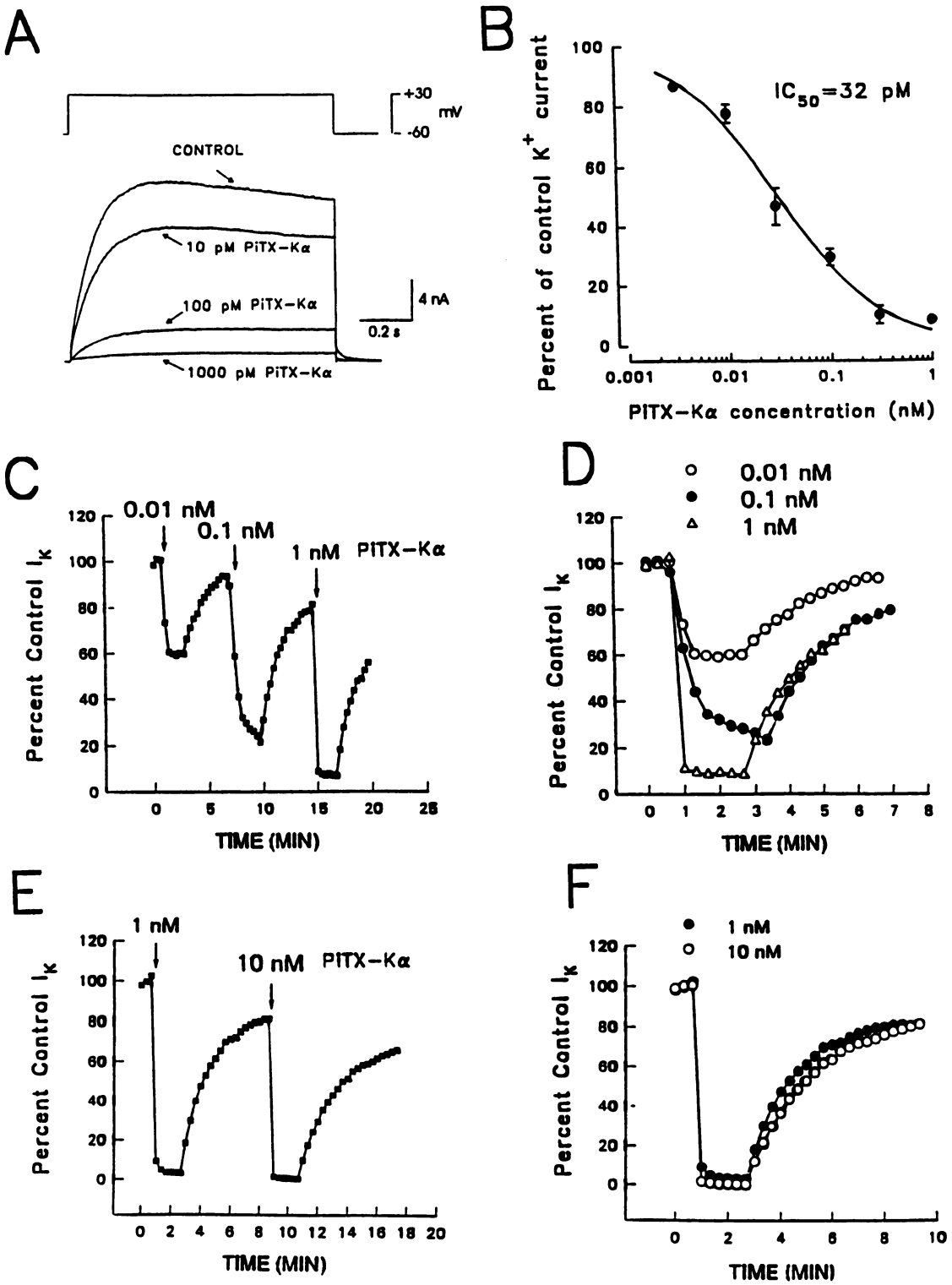

Fig. 10. Effects of PiTX-Kα on the K^+ current in patch-clamped B82 fibroblast cells transformed to express the Kv1.2 K^+ channel. A, Currents in a cell before (control) and during superfusion with increasing concentrations of PiTX-Kα. B, Concentration-response relationship for PiTX-Kα block of the K^+ current. Percentages of control values were calculated according to the formula $I_{toxin}/I_{control} \times 100$, where $I_{control}$ is the steady state current amplitude before toxin application and I_{toxin} is the steady state current amplitude during toxin application. *Points,* mean ± standard error of data from three to four cells, fit to a logistic equation for a 1:1 binding reaction (see legend to Fig. 9) with $n_H = 0.9$. C, Time course for onset and recovery from block with 0.01, 0.1, and 1 nM PiTX-Kα. The 1-sec duration depolarizing voltage steps from −60 to +30 mV were applied at 20-sec intervals. Toxin was applied for 2-min periods beginning at the points indicated (*arrows*). Steady state current amplitude was measured at the end of each depolarizing step. Percentages of control values were calculated with respect to the mean of the steady state current amplitudes during the three steps immediately before the onset of the initial toxin perfusion. D, Data from the experiment of C displayed with the percentage of control values calculated with respect to the mean of the current amplitudes for the three steps immediately before each toxin application; zero time was set at 1 min before the onset of each toxin application (recovery time constants: 106, 113, and 89 sec for 0.01, 0.1, and 1 nM PiTX-Kα, respectively). E and F, Experiment similar to those of D and E with 1 and 10 nM PiTX-Kα (recovery time constants: 106 and 147 sec).

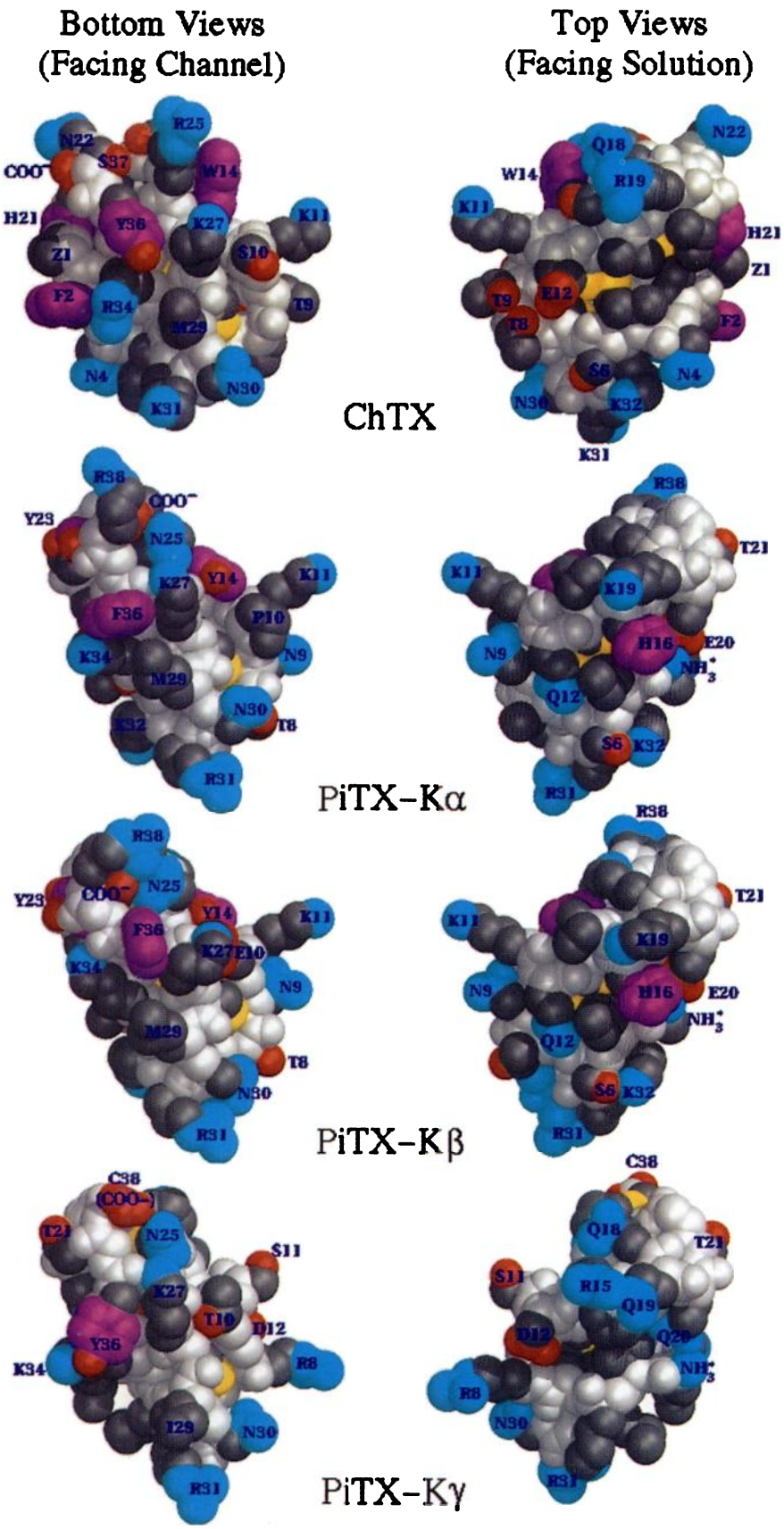

Fig. 11. Space-filling model structures of ChTX and the three PiTXs. *Right*, surfaces of the toxins that are likely (by analogy with ChTX) to face the external vestibule of the voltage-gated K^+ channel when the central Lys27 inserts into the channel pore (31). *Left*, opposite surfaces of the toxins (i.e., the surfaces that are likely to face the extracellular fluid when the toxin molecules are bound to the channel protein). *Single-letter code designations*, key amino acids and their positions (Fig. 4). Structures are color coded: *blue*, positive moieties; *red*, negative moieties; *purple*, aromatic rings; *yellow*, sulfur atoms; *dark gray*, side-chain carbons; *light gray*, peptide backbone atoms. The positively charged amino termini (NH_3^+) and negatively charged carboxyl termini (COO^-) are also indicated.

are located on this surface (Fig. 11, *bottom view*) and are believed to interact with the channel. The amino terminus of the PiTXs (Thr4 in PiTX-Kα and PiTX-Kβ and Leu4 in PiTX-Kγ) is located on the surface of the toxin that likely faces the medium (Fig. 11, *top view*).

Compared with ChTX, the PiTXs have an additional residue (Arg38 in PiTX-Kα and PiTX-Kβ and Cys38 in PiTX-Kγ) at the carboxyl terminus that is, in all cases, located on the surface of the toxin thought to interact with the channel (Fig. 11, *bottom view*, and Fig. 12). The orientation of this residue, however, differs in PiTX-Kγ compared with PiTX-Kα and PiTX-Kβ because the Cys38 of PiTX-Kγ is involved in a

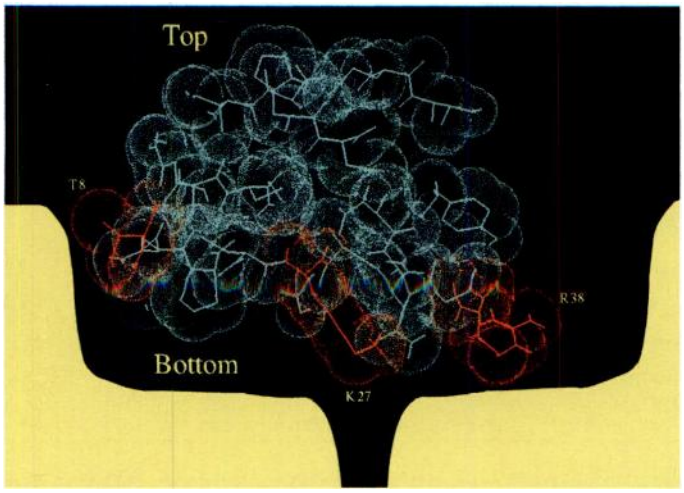

Fig. 12. Model of a cross-section through PiTX-Kα docked to a model K^+ channel. The channel protein (*yellow*) is cut through the center of the pore. The vestibule is shown as a symmetrical structure (2, 4). The toxin Lys27 is positioned so that it can protrude into the channel pore. As described for ChTX (2; see their Fig. 4), Trp8 is positioned so that it interacts with the side of the external vestibule of the channel (2). Note that Arg38 (an amino acid that is absent in ChTX) seems to be positioned to interact with the base of the channel vestibule.

disulfide bond. As in ChTX, the negatively charged terminal carboxylate of PiTX-Kγ faces the channel, whereas in PiTX-Kα and PiTX-Kβ, the positively charged Arg38 side chain probably faces the channel vestibule floor (Fig. 12).

In Table 1 are shown the amino acids in ChTX that Miller *et al.* (4) identified as critical or influential (others were designated indifferent) for the activity of the toxin as a blocker of mutated (Phe425 replaced by a glycine) *Shaker*-type voltage-gated K^+ channels (2) and Ca^{2+}-activated K^+ channels. These key amino acids are compared with those in homologous positions in the three PiTXs (Table 1 and Fig. 11). Four amino acids arrayed around the invariant Lys27 are critical to the blocking activity of ChTX against Shaker-type voltage-gated K^+ channels (Table 1); they are either identical or conservatively replaced in the PiTXs. In addition, Thr8, with a polar side chain, is present in ChTX, PiTX-Kα, and PiTX-Kβ (Fig. 4) and probably interacts with the vestibule wall (2) (Fig. 12); this moiety is replaced by a positively charged arginine in PiTX-Kγ.

Notable differences between the PiTXs and ChTX include (i) the small, polar Ser10, with hydrogen-bonding capacity, which is replaced by a nonpolar proline in PiTX-Kα, by a negatively charged glutamate in PiTX-Kβ, and by a polar threonine in PiTX-Kγ; (ii) the influential Ser24 and Ser37, which are replaced by nonpolar proline and glycine residues, respectively, in all three PiTXs; and (iii) the positively charged Arg25, which is replaced by a small, polar, but uncharged asparagine in all three PiTXs. The possible functional significance of these differences as well as the differences among the three PiTXs is discussed below.

Discussion

Three K^+ channel blockers from *P. imperator* venom. We identified, purified, and sequenced three 35-amino acid polypeptide toxins from the venom of the North African scorpion *P. imperator* that selectively block a Ca^{2+}-independent, K^+-stimulated, rapidly inactivating component of the ^{86}Rb efflux from synaptosomes. This efflux component may correspond to an inactivating (A-type), voltage-gated K^+ channel (21). The most potent of the three toxins, PiTX-Kα, inhibited the ^{86}Rb efflux (IC_{50} = 6 nM). PiTX-Kα is thus a much more potent inhibitor of this K^+ channel than is ChTX (IC_{50} = 40 nM) (24) or α-DaTX (IC_{50} = 90 nM) (23, 26), two other polypeptides that inhibit the same ^{86}Rb efflux component in synaptosomes.

PiTX-Kα is also the most potent inhibitor thus far identified of Kv1.2 channels that are stably expressed in fibroblasts (IC_{50} = 32 pM). Previous studies had indicated that this channel was inhibited by ChTX and α-DaTX with IC_{50} values in the low nanomolar range (7) and by tityustoxin-Kα with an IC_{50} value of ~210 pM (15). In contrast to reports of the relative irreversibility of *P. imperator* venom block of K^+ channels in other preparations (10, 11), the block of Kv1.2 channels in fibroblasts by PiTX-Kα was reversible. Nevertheless, the dissociation rate of PiTX-Kα ($\approx$0.01 sec^{-1}; Fig. 10) was relatively slow compared with the dissociation rates of α-DaTX and mast cell degranulating peptide in the same preparation (on the order of 0.1–1 sec^{-1}) (7).

An interesting feature of these toxins concerns their selectivity in blocking K^+ channels in synaptosomes. ChTX blocks both Ca^{2+}-activated and voltage-gated K^+ channels in several preparations (1), including synaptosomes, where it blocks the inactivating type of voltage-gated channel (24). In contrast, all three PiTXs block only the inactivating, voltage-gated K^+ channel in synaptosomes (Figs. 7 and 8). This selectivity is comparable to the selectivity of another K^+ channel toxin from the venom of *Leiurus quinquestriatus hebraeus*, toxin LqTX-K2 (12). It is apparent that the PiTXs block some inactivating (11, 12, and this report) and some noninactivating (10, 15) voltage-gated K^+ channels. This is probably not due to a lack of selectivity of the toxins but rather to specific structural features of the docking sites on the various K^+ channels. There is no *a priori* reason to expect that the structure of the K^+ channel external vestibule is linked to the structure of the inactivation gate, which may be located on the opposite (cytoplasmic) end of the channel (33). We anticipate that determination of the subunit composition of these various K^+ channels will help to resolve questions about the structural features of the channel vestibule in specific types of K^+ channels. Indeed, the toxins may be very useful tools for helping to identify the various channels (and perhaps even extracting some of them out of native membranes) and for exploring the channel structures, as exemplified by several recent studies (2–5).

PiTX-Kγ is an unusual peptide. It has a novel sequence, including a fourth pair of cysteines, and thus seems to represent a new subfamily of K^+ channel toxins.[2]

PiTX-Kγ is expressed at approximately the same level as PiTX-Kα and PiTX-Kβ, despite its very low affinity and unusual binding kinetics for the synaptosome voltage-gated, inactivating K^+ channels. Furthermore, like the other two PiTXs, it does not block either Ca^{2+}-activated K^+ channels or voltage-gated, noninactivating K^+ channels in synaptosomes. This raises the possibility that the primary acceptor for PiTX-Kγ may be a different K^+ channel. Olamendi *et al.*

[2] While this article was in preparation, Olamendi-Portugal *et al.* (34) described a toxin with an identical amino acid sequence (their toxin Pi1), which they, too, purified from *P. imperator* venom. They showed that Cys23 and Cys38 form a fourth disulfide bridge, as depicted in our model (Fig. 11).

TABLE 1
Critical and influential amino acids in ChTX and the homologous amino acids in the PiTXs

Toxin/K^+ channel target	Position											
	10	14	23	24	25	27	29	30	31	34	36	37
ChTX/Ca^{2+}-activated[a]												
Critical	Ser	Trp			Arg	Lys	Met	Asn		Arg	Tyr	
Influential												Ser
ChTX/*Shaker*[b]												
Critical						Lys	Met	Asn		Arg	Tyr	
Influential	Ser		Thr	Ser	Arg				Lys			Ser
PiTX-Kα/A-type voltage-gated	Pro	Tyr	Tyr	Pro	Asn	Lys	Met	Asn	Arg	Lys	Phe	Gly
PiTX-Kβ/A-type voltage-gated	Glu	Tyr	Tyr	Pro	Asn	Lys	Met	Asn	Arg	Lys	Phe	Gly
PiTX-Kγ/A-type voltage-gated	Thr	Gly	Cys	Pro	Asn	Lys	Ile	Asn	Arg	Lys	Tyr	Gly

[a] From Stampe *et al.* (4).
[b] These data refer to a mutant *Shaker* K^+ channel (F425G), with a bulky phenylalanine in position 425 replaced by a smaller glycine to enhance ChTX binding by ~3 orders of magnitude. From Goldstein *et al.* (2).

(34) reported that PiTX-Kγ blocks *Shaker* B K^+ channels with relatively high affinity (IC_{50} = <70 nM), but this is ~3 orders of magnitude lower affinity than that of PiTX-Kα for the Kv1.2 channel (Fig. 10B).

Modeling of toxin structures; structure-activity relationships. The NMR solution structures of a number of K^+ channel toxins from scorpion venoms have been determined; these include ChTX (17, 18, 35), iberiotoxin (36), margatoxin (5, 37), kaliotoxin (5, 28), agitoxin-2 (38), and noxiustoxin (27). All of these peptides have the same type of structure: they are compact molecules with an antiparallel, three-stranded β sheet on one face and an α helix on the other. This structure is stabilized by three disulfide bonds that make up most of the interior core, whereas the other amino acid side chains are on the molecule surface.

We used the molecular coordinates from ChTX and the CHARMm and QUANTA programs to model the structures of the three PiTXs. The modeled structure for PiTX-Kα (Fig. 11) is largely consistent with the preliminary NMR structure (39). This implies that the modeling methods based on previously published homologous structures are reasonable. Comparison of our results with the published NMR structures of the homologous toxins indicates that apparently all of these small K^+ channel toxins from scorpion venoms are folded similarly. The main differences between the toxin structures, which likely account for toxin selectivity, must therefore reside in specific features of the side groups that extend from the backbone, as well as in the precise location of surface charges. In this respect, the absence of the first three influential amino acids of ChTX (PyroGlu1, Phe2, and Thr3) and the critical positively charged Arg25 (replaced by a polar asparagine) in the PiTXs (Table 1) may be responsible for the inability of the PiTXs to block Ca^{2+}-activated K^+ channels (Fig. 7) (4). Conversely, the identity or conservative replacement (Table 1) of the amino acids at all five critical positions for the Shaker K^+ channel-blocking activity of ChTX (2) may account for the ability of all three PiTXs to block voltage-gated, inactivating K^+ channels in synaptosomes (Figs. 6 and 8). This would also explain the effectiveness of PiTX-Kα (the only PiTX available for testing) on voltage-gated Kv1.2 channels (Fig. 10).

The single amino acid substitution between PiTX-Kα (Pro10, a nonpolar helix breaker) and PiTX-Kβ (Glu10, a small acidic helix former) must account for the 7-fold difference in potency (Fig. 9). The models (Fig. 11) show that the key Lys27 lies close to the amino acid at position 10 in both PiTXs. In PiTX-Kβ, however, the positive charge on Lys27 may be influenced by the negative charge on Glu10, so there may be some charge neutralization; this would not occur with the nonpolar Pro10 in PiTX-Kα. Alternatively, a small change in the backbone structure, which is not evident in the model, could account for the difference in potency. This uncertainty may be resolved by determining and comparing the NMR solution structures of these two toxins.

It is less clear why PiTX-Kγ is so much less potent in blocking voltage-gated, inactivating K^+ channels in synaptosomes (Fig. 9). It seems reasonable, however, that the absence of an aromatic side chain in position 14 and the replacement of Arg38 may play key roles because these amino acids are exposed on the bottom (docking) surface (Fig. 11). In PiTX-Kα and PiTX-Kβ, the positively charged side chain of Arg38 faces the binding surface of the channel, whereas in PiTX-Kγ, the negatively charged carboxyl-terminal carboxyl group occupies this position (Fig. 11). This analysis suggests that comparison of the spatial relationships among the side groups surrounding Lys27 in the various scorpion K^+ channel toxins with their selectivities and affinities will provide new insight into their structure-function relationships.

References

1. Miller, C. The charybdotoxin family of K^+ channel-blocking peptides. *Neuron* **15:**5–10 (1995).
2. Goldstein, S. A. N., D. J. Pheasant, and C. Miller. The charybdotoxin receptor of a *Shaker* K^+ channel: peptide and channel residues mediating molecular recognition. *Neuron* **12:**1377–1388 (1994).
3. Hidalgo, P., and R. MacKinnon. Revealing the architecture of a K^+ channel pore through mutant cycles with a peptide inhibitor. *Science (Washington D. C.)* **268:**307–310 (1995).
4. Stampe, P., L. Kolmakova-Partensky, and C. Miller. Intimations of K^+ channel structure from a complete functional map of the molecular surface of charybdotoxin. *Biochemistry* **33:**443–450 (1994).
5. Aiyar, J., J. M. Withka, J. P. Rizzi, D. H. Singleton, G. C. Andrews, W. Lin, J. Boyd, D. C. Hanson, M. Simon, B. Dethlefs, C. Lee, J. E. Hall, G. A. Gutman, and K. G. Chandy. Topology of the pore-region of a K^+ channel revealed by the NMR-derived structures of scorpion toxins. *Neuron* **15:** 1169–1181 (1995).
6. Carbone, E., E. Wanke, G. Prestipino, L. D. Possani, and A. Maelicke. Selective blockage of voltage-dependent K^+ channels by a novel scorpion toxin. *Nature (Lond.)* **296:**90–91 (1982).
7. Werkman, T. R., T. Kawamura, S. Yokoyama, H. Higashida, and M. A. Rogawski. Charybdotoxin, dendrotoxin and mast cell degranulating peptide block the voltage-activated K^+ current of fibroblast cells stably transfected with NGK1 (Kv1.2) K^+ channel complementary DNA. *Neuroscience* **50:**935–946 (1992).
8. Garcia-Calvo, M., R. J. Leonard, J. Novick, S. P. Stevens, W. Schmalhofer, G. J. Kaczorowski, and M. L. Garcia. Purification, characterization, and biosynthesis of *Centruroides magaritatus* venom that selectively inhibits

voltage-dependent potassium channels. *J. Biol. Chem.* **268:**18866–18874 (1993).
9. Miller, C. Diffusion-controlled binding of a peptide neurotoxin to its K^+ channel receptor. *Biochemistry* **29:**5320–5325 (1990).
10. Pappone, P. A., and M. D. Cahalan. *Pandinus Imperator* scorpion venom blocks voltage-gated potassium channels in nerve fibers. *J. Neurosci.* **7:**3300–3305 (1987).
11. Pappone, P. A., and M. T. Lucero. *Pandinus imperator* scorpion venom blocks voltage-gated potassium channels in GH_3 cells. *J. Gen. Physiol.* **91:**817–833 (1988).
12. Blaustein, M. P., R. S. Rogowski, M. J. Schneider, and B. K. Krueger. Polypeptide toxins from the venoms of old world and new world scorpions preferentially block different potassium channels. *Mol. Pharmacol.* **40:** 932–942 (1991).
13. Schägger, H., and G. von Jagow. Tricine-sodium dodecyl sulfate-polyacrylamide gel electrophoresis for the separation of proteins in the range from 1 to 100 kDa. *Anal. Biochem.* **166:**368–379 (1987).
14. Park, C. S., S. F. Hausdorff, and C. Miller. Design, synthesis, and functional expression of a gene for charybdotoxin, a peptide blocker of K^+ channels. *Proc. Natl. Acad. Sci. USA* **88:**2046–2050 (1991).
15. Werkman, T. R., T. A. Gustafson, R. S. Rogowski, M. P. Blaustein, and M. A. Rogawski. Tityustoxin-Kα, a structurally novel and highly potent K^+ channel peptide toxin, interacts with the α-dendrotoxin binding site on the cloned Kv1.2K^+ channel. *Mol. Pharmacol.* **44:**430–436 (1993).
16. Howell, M. L., and K. M. Blumenthal. Cloning and expression of a synthetic gene for *Cerebratulus lacteus* neurotoxin B-IV. *J. Biol. Chem.* **264:** 15268–15273 (1989).
17. Bontems, F., C. Roumestand, P. Boyot, B. Gilquin, Y. Doljansky, A. Menez, and F. Toma. Three-dimensional structure of natural charybdotoxin in aqueous solution by ^{1}H-NMR: charybdotoxin possesses a structural motif found in other scorpion toxins. *Eur. J. Biochem.* **196:**19–28 (1991).
18. Bontems, F., C. Roumestand, B. Gilquin, A. Menez, and F. Toma. Refined structure of charybdotoxin: common motifs in scorpion toxins and insect defensins. *Science (Washington D. C.)* **254:**1521–1523 (1991).
19. Loret, E. P., R. M. del Valle, P. Mansuelle, F. Sampieri, and H. Rochat. Positively charged amino acid residues located similarly in sea anemone and scorpion toxins. *J. Biol. Chem.* **269:**16785–16788 (1994).
20. Bontems, F., B. Gilquin, C. Roumestand, A. Menez, and F. Toma. Analysis of side-chain organization on a refined model of charybdotoxin: structural and functional implications. *Biochemistry* **31:**7756–7764 (1992).
21. Bartschat, D. K., and M. P. Blaustein. Potassium channels in isolated presynaptic nerve terminals from rat brain. *J. Physiol.* **361:**419–440 (1985).
22. Bartschat, D. K., and M. P. Blaustein. Calcium-activated potassium channels in isolated presynaptic nerve terminals from rat brain. *J. Physiol.* **361:**441–457 (1985).
23. Benishin, C. G., R. G. Sorensen, W. E. Brown, B. K. Krueger, and M. P. Blaustein. Four polypeptide components of green mamba venom selectively block certain potassium channels in rat brain synaptosomes. *Mol. Pharmacol.* **34:**152–159 (1988).
24. Schneider, M. J., R. S. Rogowski, B. K. Krueger, and M. P. Blaustein. Charybdotoxin blocks both Ca-activated K channels and Ca-independent voltage-gated K channels in rat brain synaptosomes. *FEBS Lett.* **250:**433–436 (1989).
25. Nachshen, D. A., and M. P. Blaustein. The effects of some organic "calcium antagonists" on calcium influx in presynaptic nerve terminals. *Mol. Pharmacol.* **16:**579–586 (1979).
26. Rogowski, R. S., B. K. Krueger, J. H. Collins, and M. P. Blaustein. Tityustoxin-Kα blocks voltage-gated, non-inactivating K^+ channels and unblocks inactivating K^+ channels by α-dendrotoxin in synaptosomes. *Proc. Natl. Acad. Sci. USA* **91:**1475–1479 (1994).
27. Dauplais, M., B. Gilquin, L. D. Possani, R. Gurrola-Briones, C. Roumestand, and A. Menez. Determination of the three-dimensional solution structure of noxiustoxin: analysis of structural differences with related short-chain scorpion toxins. *Biochemistry* **34:**16563–16573 (1995).
28. Fernandez, I., R. Romi, S. Szendeffy, M. F. Martin-Eauclaire, H. Rochat, J. Van Rietschoten, M. Pons, and E. Giralt. Kaliotoxin (1–37) shows structural differences with related potassium channel blockers. *Biochemistry* **33:**14256–14263 (1994).
29. Lebreton, F., M. Delepierre, A. M. Ramírez, C. Balderas, and L. D. Possani. Primary and NMR three-dimensional structure determination of a novel crustacean toxin from the venom of the scorpion *Centruroides limpidus limpidus* Karsch. *Biochemistry* **33:**11135–11149 (1994).
30. Olivera, B. M., D. R. Hillyard, M. Marsh, and D. Yoshikami. Combinatorial peptide libraries in drug design: lessons from venomous cone snails. *Trends Biotech.* **13:**422–426 (1995).
31. Park, C.-S., and C. Miller. Interaction of charybdotoxin with permeant ions inside the pore of a K^+ channel. *Neuron* **9:**307–313 (1992).
32. Naini, A. A., and C. Miller. A symmetry-driven search for electrostatic interaction partners in charybdotoxin and a voltage-gated K^+ channel. *Biochemistry* **35:**6181–6187 (1996).
33. Isacoff, E. Y., Y. N. Jan, and L. Y. Jan. Putative receptor for the cytoplasmic inactivation gate in the *Shaker* K^+ channel. *Nature (Lond.)* **353:**86–90 (1991).
34. Olamendi-Portugal, T., F. Gomez-Lagunas, G. B. Gurrola, and L. D. Possani. A novel structural class of K^+ channel blocking toxin from the scorpion: *Pandinus imperator*. *Biochem. J.* **315:**977–981 (1996).
35. Kobayashi, Y., H. Takashima, H. Tamaoki, Y. Kyogoku, P. Lambert, H. Kuroda, N. Chino, T. X. Watanabi, T. Kimura, S. Sakakibara, and L. Moroder. The cystine-stabilized α-helix: a common structural motif of ion-channel blocking neurotoxic peptides. *Biopolymers* **31:**1213–1220 (1991).
36. Johnson, B. A., and E. E. Sugg. Determination of the three-dimensional structure of iberiotoxin in solution by ^{1}H nuclear magnetic resonance spectroscopy. *Biochemistry* **31:**8151–8159 (1992).
37. Johnson, B. A., S. P. Stevens, and J. M. Williamson. Determination of the three-dimensional structure of margatoxin by ^{1}H, ^{19}C, ^{15}N triple-resonance nuclear magnetic resonance spectroscopy. *Biochemistry* **33:** 15061–15070 (1994).
38. Krezel, A. M., C. Kasibhatla, P. Hidalgo, R. MacKinnon, and G. Wagner. Solution structure of the potassium channel inhibitor agitoxin 2: caliper for probing channel geometry. *Prot. Sci.* **4:**1478–1489 (1995).
39. Tenenholz, T., R. S. Rogowski, J. C. Amburgey, J. C. Collins, T. A. Gustafson, M. P. Blaustein, and D. J. Weber. Sequence-specific assignments and secondary structure determination of a toxin from *Pandinus imperator* (PiTX-Kα) using NMR spectroscopy. *Biophys. J.* **70:**A59 (1996).
40. Giminez-Gallego, G., M. A. Navia, J. P. Rubin, G. M. Katz, G. J. Kaczorowski, and M. L. Garcia. Purification, sequence, and model structure of charybdotoxin, a potent selective inhibitor of calcium-activated potassium channels. *Proc. Natl. Acad. Sci. USA* **85:**3329–3333 (1988).

Send reprint requests to: Dr. Mordecai P. Blaustein, Department of Physiology, University of Maryland School of Medicine, 655 West Baltimore Street, Baltimore, MD 21201. E-mail: mblauste@umabnet.ab.umd.edu